Journal of Power Sources 196 (2011) 5223–5230

Contents lists available at ScienceDirect

Journal of Power Sources

journal homepage: www.elsevier.com/locate/jpowsour

Electrolyte infiltration in phosphazene-based dye-sensitized solar cells

Shih-To Fei [a], Seung-Hyun Anna Lee [a], Sean M. Pursel [b], James Basham [c], Andrew Hess [a], Craig A. Grimes [c], Mark W. Horn [b], Thomas E. Mallouk [a], Harry R. Allcock [a,*]

[a] Department of Chemistry, The Pennsylvania State University, University Park, PA 16802, United States
[b] Department of Engineering Science and Mechanics, The Pennsylvania State University, University Park, PA 16802, United States
[c] Department of Electrical Engineering, The Pennsylvania State University, University Park, PA 16802, United States

ARTICLE INFO

Article history:
Received 11 January 2011
Accepted 13 January 2011
Available online 26 January 2011

Keywords:
Dye sensitized solar cells
Electrolyte
Phosphazene
Polyphosphazene
Nano-structured surface

ABSTRACT

We report here a study of phosphazene polymer and oligomer electrolyte infiltration into high surface area titanium dioxide electrodes and its effect on the performance of dye-sensitized solar cells. The effects of different cell assembly procedures on the electrochemical properties are examined, as well as the infiltration of electrolytes based on poly[bis(2-(2-methoxyethoxy)ethoxy)phosphazene] (MEEP), hexakis(2-(2-methoxyethoxy)ethoxy)cyclotriphosphazene (MEE trimer), and a linear short chain analogue into conventional titanium dioxide electrode mesoporous (nanosphere) films, microcolumns and nanowires. The effects of temperature, co-solvents, and the order of addition of the electroactive components are found to affect both the conductivity of the electrolytes and the electrochemical performance of the cells. Cross-sectional scanning electron microscopy (SEM) imaging is employed to examine the degree of electrolyte infiltration into the nanostructured electrodes as a function of filling conditions. Using these techniques, conditions are identified for achieving a high degree of pore filling by the three electrolyte systems. Increased power conversion efficiency is obtained when iodine is introduced after the heating and evacuation procedures required for maximum infiltration.

1. Introduction

In this paper we report an investigation of electrolyte infiltration into two types of nanostructured titania electrodes, and the effect of different infiltration methods on the performance of polymer–electrolyte dye-sensitized solar cells (DSSCs). Solar cells, or photovoltaic cells, are devices capable of generating electricity directly when exposed to sunlight [1,2]. Photovoltaic cells have long been regarded as one of the ultimate "green energy" options [3,8]. However, a major challenge in the widespread implementation of a solar energy economy is that the cost of solar electricity is currently about 5–20 times that of conventional power [4–8]. To overcome this problem, a number of alternative solar cell designs have been introduced [9–15]. One of the most promising inexpensive photovoltaic cells is the dye-sensitized solar cell (DSSC) [12]. This type of device uses a layer of nano-scale semiconductor particles (usually titanium oxide), fused into a mesoporous film and stained with light absorbing dyes, which inject electrons into the transparent porous semiconductor film when the dye is excited by light. An electrolyte layer (commonly an I^-/I_3^- mixture dissolved in a liquid electrolyte) is present to provide a complete circuit between the photoanode and dark cathode [11–13].

Two of the most important factors that limit the performance of a dye-based cell are the conductivity of the electrolyte, and the volatility of the small molecule organic solvents normally used as the electrolyte medium. The necessity of sealing DSSCs with liquid electrolytes also increases the complexity and cost of manufacturing. The fluidity of the electrolyte and volatility at elevated temperatures means that even minor physical damage incurred after installation could lead to significant loss of electrolyte and thus high failure rates and reduced cell lifetime. A number of non-volatile electrolytes including ionic liquids, small molecule substitutes, and polymeric components have been investigated to address this problem with various degrees of success [11,16–19].

Abbreviations: AC, alternating current; A_c, geometric surface area of cell; AM 1.5, reference solar spectral irradiance:air mass 1.5; ASTM, American Society for Testing and Materials; BSE, backscattered electron; DC, direct current; DSSC, dye-sensitized solar cell; DSSCs, dye-sensitized solar cells; EDS, energy dispersive spectroscopy; *ff*, fill-factor; FTO, fluorine-doped tin oxide; I_0, input light irradiance; J_{sc}, short circuit current; MCL, Materials Characterization Laboratory; MEE trimer, hexakis(2-(2-methoxyethoxy)ethoxy)cyclotriphosphazene; MEE, 2-(2-methoxyethoxy)ethoxy side unit; MEEP, poly(bis(2-(2-methoxyethoxy)ethoxy)phosphazene); *n*, cell-efficiency; nc-TiO_2, titanium dioxide nanoparticles; NMR, nuclear magnetic resonance; P_m, maximum power output of cell; PMII, 1-propyl-3-methylimidazolium iodide; SEM, scanning electron microscopy; tBuPy, para-tert-butyl pyridine; T_g, glass transition temperature; THF, tetrahydrofuran; V_{oc}, open circuit voltage.

* Corresponding author. Tel.: +1 814 865 3527.
E-mail address: hra@chem.psu.edu (H.R. Allcock).

0378-7753/$ – see front matter © 2011 Elsevier B.V. All rights reserved.
doi:10.1016/j.jpowsour.2011.01.052

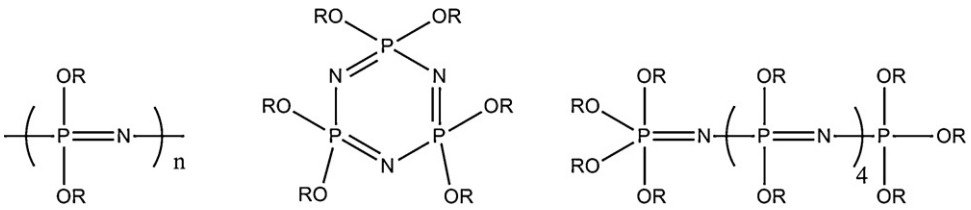

1 2 3

OR = $O(CH_2CH_2O)_2CH_3$ = MEE side unit

Fig. 1. Structure of phosphazenes with oligoethyleneoxy side chains [24]. Compound **1** is poly(bis(2-(2-methoxyethoxy)ethoxy)phosphazene) (MEEP), where the value of *n* can be as high as 15,000. Compound **2** is hexakis(2-(2-methoxyethoxy)ethoxy)cyclotriphosphazene (MEE trimer). A short chain analogue of **1**, with four repeating units and two terminal phosphorus atoms bearing MEE side units was also studied and is designated as compound **3**.

Use of a solid polymer electrolyte is a possible solution to this problem [18,19]. Solid polymer electrolyte systems offer high dimensional stability, ease of processing, and very low volatility. However, the main disadvantage of solid (unplasticized) polymer electrolytes is the low ionic conductivity brought about by limited ion mobility in the solid matrix of even the most flexible polymers. Moreover, the TiO_2 layers used in most dye solar cells are made by the stacking of spherical nanocrystals. This results in a porous anode with random and tortuous channels only a few nanometers wide (2–15 nm pore size). Ideally, the electrolyte should be in contact with the entire dye-functionalized TiO_2 surface. However, this is difficult for polymer electrolytes because the twisted narrow channels require the polymer molecules to uncoil before they can enter the pores. This entropically unfavorable process makes full contact of the electrolyte with the TiO_2 surface and the dye molecules difficult to achieve, and is often a major contributor to the low efficiency of solid polymeric DSSCs compared to gel (plasticized) or liquid electrolyte systems [20–23].

The ideal polymer electrolyte for nanopore infiltration should be fully amorphous and flexible enough at the molecular level to allow dissolved ions to migrate from one polymer molecule to another, facilitated by the thermally induced movements of the flexible chains. Previous studies have shown that polymer electrolytes with very good ion-conducting properties, such as those with oligoethylene oxide side chains (Fig. 1) [24–26] can be synthesized by linking ionically conductive side chains to a flexible polyphosphazene backbone. This approach provides access to amorphous polymers with good thermal and photo-stability [24]. Another important advantage of these polyphosphazenes over other polymers is the low glass transition temperature and the total absence of crystallinity. Thus, they retain high internal mobility even at low temperatures due to the unusually high torsional freedom of the P–N backbone. This leads to gum-type materials that, in addition to having faster ion transport than, for example poly(ethylene oxide) (PEO), have the potential to penetrate and adhere to complex surface structures. The excellent performance of these polymer electrolytes in lithium batteries [24–26] suggests that they might also be good electrolytes for DSSCs. However, in the case of the DSSC, conduction of anions such as I^-/I_3^- is required as opposed to conduction of cations such as Li^+.

The problem of polymer penetration into a nanosphere-based electrode have stimulated consideration of alternative approaches. Semiconductor nanorod "bed of nails" arrays have been suggested as the optimum electrode geometry. This geometry should increase overall cell efficiency by minimizing the diffusion length of both the electrons within the TiO_2 and the charge carriers in the electrolyte since it eliminates the tortuosity of the channels that occur in nanosphere-based electrodes [27]. By organizing surface nanorods to produce wide, straight channels, it should be possible to promote the infiltration of oligomers and polymers into the pores of the array and thus generate a large contact area. A comparison of polymer or oligomer infiltration into TiO_2 nanosphere and nanorod arrays with different channel sizes, rod shapes, orientations, or surface morphologies should suggest optimum approaches to higher efficiency dye-cells [28]. In this work, the different electrolytes were examined for infiltration into both conventional nanosphere and structured nanorod assemblies, and the conductivity of the electrolytes and the corresponding cell efficiencies under various assembly conditions were measured by AC impedance and DC current–voltage techniques. Pore-filling by the polymer or oligomer electrolyte was visualized through cross-sectional SEM studies and was correlated with the electrochemical data.

2. Materials and methods

2.1. Materials

The starting material for nearly all phosphazene reactions, hexachlorocyclotriphosphazene $(NPCl_2)_3$, was obtained from Fushimi Chemical and Pharmaceutical Co. Ltd. (Japan). This small-molecule cyclic compound was purified by recrystallization from heptane, and sublimation at 40 °C under 0.05 mmHg vacuum. Celite, sodium metal, anhydrous lithium iodide, 1-propyl-3-methyl-imidazolium iodide (PMII), iodine, di(ethylene glycol)methyl ether, anhydrous acetonitrile, ethanol, and tert-butanol were obtained from Sigma–Aldrich (St. Louis, MO). Diethyl ether, hexanes, tetrahydrofuran (THF), and methylene chloride (CH_2Cl_2) were purchased from VWR (Radnor, PA). N-719 dye (a ruthenium bipyridyl derivative), fluorine-doped tin oxide (FTO) glass, and titanium dioxide nanoparticles (nc-TiO_2) were obtained from Solaronix (Aubonne, Switzerland). Di(ethylene glycol) methyl ether was purified by vacuum distillation after drying over calcium hydride. The diethyl ether, hexanes, THF, and CH_2Cl_2 were purified through copper/silica catalytic drying columns. All other chemicals were used as received.

2.2. Characterization

Compounds were characterized by ^1H and ^{31}P NMR spectroscopy using a Bruker (Billerica, MA) AMX-360 instrument. Molecular weight of polymers was measured using gel-permeation chromatography (GPC) and a Hewlett–Packard (Palo Alto, CA) 1047A refractive index detector and two Phenomenex (Torrance, CA) Phenogel linear 10 columns. GPC samples were eluted at a rate of 1.0 mL min^{-1} with a 10 mM solution of tetra-*n*-butylammonium nitrate in THF. The elution times were calibrated with polystyrene standards. Alternating current (AC) conductivity measurements were made using a HP-4192A impedance analyzer and a two-

point liquid or solid conductivity cell. The effective conductivity of each electrolyte was then calculated based on an equivalent circuit model assuming ionic mass-transport as the limiting factor [29]. Photocurrent and photovoltage measurements were obtained from test cells using a Keithley (Cleveland, OH) 2400 source meter and an Oriel (Irvine, CA) 77250 150 W Xe lamp fitted with an AM 1.5 filter. SEM studies were carried out using an FEI Philips (Hillsboro, OR) XL-20 instrument at the Materials Characterization Laboratory (MCL) at Penn State.

2.3. Synthesis of poly(bis(2-(2-methoxyethoxy)ethoxy) polyphosphazene) (MEEP) and hexakis(2-(2-methoxyethoxy) ethoxy)cyclotriphosphazene (MEE trimer)

These syntheses were based on previous literature reports with no modification [30,31]. The molecular weight of the MEEP polymer was 5.0×10^5 as measured by gel-permeation chromatography.

2.4. Synthesis of short-chain oligo(bis(2-(2-methoxyethoxy) ethoxy)polyphosphazene) **(3)**

Synthesis of a short chain chlorophosphazene with six phosphorus atoms was carried out according to a previous literature report [32]. Replacement of the chlorine atoms by the MEE-type groups was accomplished in the same way as for the MEEP high polymer by replacement of the chlorine atoms using the sodium salt of the etheric alcohol [33]. This compound was terminated at one end by a $P(MEE)_3$ unit and by a $P(MEE)_4$ unit at the other.

2.5. Electrolyte solution mixture preparation

In a typical experiment, MEEP polymer (0.1 g) was dissolved in acetonitrile (5 mL) with an appropriate ratio of LiI to I_2. The solution was stirred overnight to ensure complete mixing, and was used directly in the assembly of DSSCs. For ionic conductivity experiments, the same sample solution was freed from solvents either by evaporation under atmospheric conditions for 60 h, under vacuum conditions for 1 h or 16 h, or at 60 °C for 1 h or 16 h.

2.6. Electrode fabrication

Nanoparticle-based nanoporous titanium oxide electrodes were fabricated based on modified published procedures [11,34]. Transparent FTO-glass substrates (2.5 cm × 2.5 cm) were pre-treated by immersion in isopropanol and sonication for 20 min, followed by 20 min sonication in ethanol. The substrate was then rinsed with deionized water and air-dried. A few drops of nanocrystalline (nc) TiO_2 paste, formulated by previously reported procedures [34], were spread onto the conductive side of the FTO-glass using a doctor blade. Adhesive tape spacers were applied to opposite edges of the electrode to control the thickness of the doctor-bladed nc-TiO_2 films. The samples were then sintered at 475 °C for 30 min and cooled to 150 °C in dry air, followed by immediate immersion in a 0.3 mM solution of N-719 dye in a mixture of acetonitrile and tert-butanol (50:50). The films were sensitized at room temperature for 48 h before being rinsed with acetonitrile to remove excess dye. Comparison samples of identical TiO_2 structures fabricated on silicon wafers were also prepared for SEM studies in order to eliminate possible complications caused by stress during cross-section fracture. Nanocolumn-based titanium oxide substrates and nanoparticle electrodes were fabricated on silicon wafers for SEM studies following published procedures [11,28,34,35].

2.7. Test solar cell assembly

The electrolyte was applied to each TiO_2 electrode via solution casting. A spacer made from stretched Parafilm (thickness ≈ 40 μm) was applied around the perimeter of the TiO_2 layer. Four drops of the acetonitrile–MEEP solution were then applied to the 5 mm × 5 mm electrode surface and allowed to dry in air for 30 min, and the process was repeated until the thickness of the polymer film matched that of the spacer. The assembly was then allowed to dry further under appropriate conditions as described below for each of the experiments. The platinum counter-electrode was assembled on top of the electrolyte layer and clamped in place before carrying out a standard photo-conversion efficiency characterization evaluation with conditions defined in ASTM G-173-03 for air mass (AM) 1.5, 1000 W m^{-2} irradiation.

2.8. SEM scans for cross-section of MEEP–TiO_2 infusions

MEEP polymer was solution-cast (0.15 g dissolved in 5 mL of acetone) onto nanoporous TiO_2 on FTO-coated glass or Si wafer substrates by the procedure described above. Each sample was dried overnight under either atmospheric pressure or vacuum conditions, and at either room temperature or 60 °C. The polymer was then crosslinked by exposure to a 20 Mrad gamma radiation dose from a ^{60}Co source at the Pennsylvania State University Breazeale Nuclear Reactor facility, and then frozen in liquid nitrogen before being fractured on the edge with a glass-cutter. The cross section was gold-sputtered before SEM analysis to ensure high quality imaging, except for energy dispersive spectroscopy (EDS) and backscattered electron (BSE) runs that operated under low-vacuum settings.

3. Results and discussion

3.1. Viability of MEEP phosphazene polymer as a solar cell electrolyte component

An objective of this research was to understand the effect of electrolyte infiltration on the performance of the DSSC. As mentioned, the classical design of a dye solar cell and experimental experience with polymer electrolytes implied that a high molecular weight polymer electrolyte would not easily infiltrate a nanosphere based electrode. Poor infiltration would result in a low level of dye utilization because much of the dye-coated TiO_2 surface would not be in contact with the polymer electrolyte phase. Thus, only a fraction of the photoelectron-generating dye molecules would be regenerated by the electrolyte after injecting an electron into the TiO_2. This would lead to either rapid back-electron transfer from TiO_2 to the dye, or would cause oxidative degradation of the dye – both of which would lead to lower photocurrent and poorer performance of the solar cell.

By using a low-T_g polymer as a polymer electrolyte, it was anticipated that the degree of electrolyte infiltration could be controlled by changing the cell fabrication conditions. For example, the application of heat during the process should lead to better infiltration by lowering the viscosity of the electrolyte. The current–voltage characteristics of each assembled cell could then be obtained, and any trends cross-checked by ion conductivity measurements of the electrolyte after different processing conditions. Moreover, the penetration of the electrolyte into the electrode surface can be monitored by cross-sectional SEM analysis of the polymer–electrode assembly. In this way it should be possible to distinguish between variations in cell performance that result from a change in electrolyte infiltration or from changes in the conduction properties of the electrolyte itself.

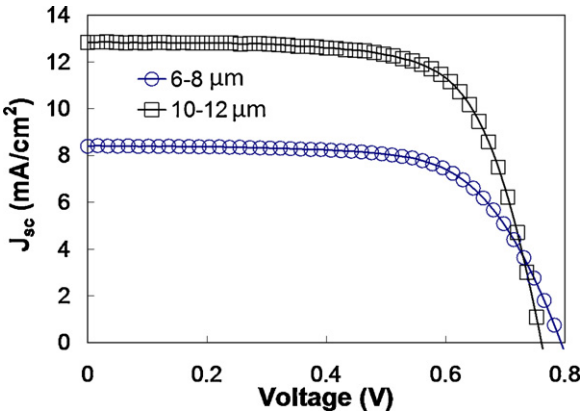

Fig. 2. *J–V* characteristics of conventional DSSCs with an acetonitrile based electrolyte that contained 0.1 M LiI, 0.6 M 1,2-dimethyl-3-hexylimidazolium iodide, 0.05 M I_2, 0.5 M 4-*tert* butylpyridine, and 0.1 M guanidinium isothiocyanate. (A) The thickness of the TiO_2 film was 6–8 μm. (B) The thickness of the TiO_2 film was 10–12 μm.

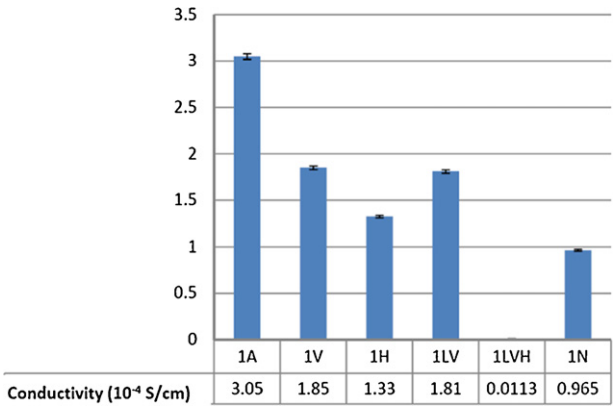

Fig. 3. AC conductivity results for sample 1 containing 1:1:10 LiI:I_2:MEEP (by mass) under different solvent removal conditions. Sample 1A: solvent removed under dry atmospheric conditions for 16 h. Sample 1H: solvent removed under heating for 1 h. Sample 1V: solvent removed under reduced pressure for 1 h. Sample 1LV: solvent removed under reduced pressure for 16 h. Sample 1LVH: solvent removed under reduced pressure and heating for 16 h. Sample 1N: solvent removed under reduced pressure and heating before application of I_2. All data points are the average of at least 6 runs with standard deviation around 1%. Error bar for sample 1LVH is too small to show on graph.

The single-cell energy conversion efficiency η is the percentage of light energy converted into electrical energy, as defined by the equation $\eta = 100(P_{max}/(I_0 A_c))$, where P_{max} is the maximum power output of the cell, I_0 is the input light irradiance, and A_c is the geometric surface area of the cell.

All of the photovoltaic data was acquired under 1 Sun intensity. The benchmark cells, to which the polymer electrolyte DSSCs were compared, contained a conventional acetonitrile electrolyte and a nanosphere-TiO_2 electrode system sensitized by the N719 dye. These control cells from our own laboratory gave 5–6.5% ($A_c = 0.25\ cm^2$) efficiency reproducibly under AM 1.5 irradiation. Fig. 2 and Table 1 show the photovoltaic measurements of conventional DSSCs of different TiO_2 thickness using liquid electrolytes. Generally, 10–12 μm TiO_2 films are required to effectively absorb all of the incident photons since increases in TiO_2 film thickness provides more dye molecules for photon absorption. This results in increases in J_{sc} but the V_{oc} also begins to decrease due to an increased dark current. The highest reported efficiency of Ru-based DSSCs with liquid electrolyte is 11.5% [13]. By contrast, most polymer electrolyte dye cells reported in the literature have ≤1% efficiency under the same conditions [18,19].

3.2. Influence of residual solvent in the electrolyte

A variety of MEEP-based solar cell electrolytes were formulated by dissolving the polymer together with an iodide salt and iodine in either acetone or acetonitrile and then evaporating the solvent until a dry, even film was formed on the electrode surface of the test cell. The efficiencies for nanocrystalline film dye cell assemblies as well as the AC ionic conductivities of these electrolytes are listed in Fig. 3.

Ideally, the solvent should be removed before the cell is assembled in order to increase the mechanical stability of the electrolyte. However, solvent removal by heat and/or vacuum can lead to variability in the cell efficiency. For instance, the highest cell efficiency obtained during preliminary studies was 3% when using a MEEP electrolyte that was drop-cast onto the electrode surface using acetonitrile as the solvent followed by solvent evaporation, and a number of other samples also showed efficiencies above 2%. However, these results were highly variable and under more controlled solvent removal conditions cell efficiencies below 1% were obtained. It is suspected that the higher efficiencies are due to a solvent retention effect – i.e., the "dried" polymer electrolyte behaved more like a gel electrolyte with the organic solvent trapped in the polymer matrix acting as a plasticizer.

Analysis of the electrolyte sample compositions by NMR spectroscopy support this suspicion by indicating that up to 8% of the solvent (molar concentration relative to one repeating unit of polymer) remained after 120 h of room temperature drying under atmospheric conditions. Solvent-removal under different conditions was also monitored by ionic conductivity measurements [29]. The results are summarized in Fig. 3. As shown, most of the solvent-removal conditions led to similar decreases in conductivity, which matched the NMR observation that 4–5% of the solvent still remained. Only when both heat and reduced pressure were applied for extended periods of time (which resulted in a significant decrease in the conductivity), did the NMR analysis fail to detect residual solvent.

Table 1
Photovoltaic parameters of DSSCs with different TiO_2 nanosphere layer thickness with an acetonitrile based electrolyte. The number of samples tested under the same conditions is shown in parentheses.

Sample	V_{oc} (V)	J_{sc} (mA cm^{-2})	*ff*	η (%)
6–8 μm (4)	0.78 ± 0.01	8.4 ± 0.4	0.67 ± 0.01	4.4 ± 0.2
10–12 μm (5)	0.761 ± 0.004	12.8 ± 0.7	0.696 ± 0.008	6.8 ± 0.4

3.3. Iodine volatilization

The decrease in mass after drying the electrolytes could not be fully accounted for by loss of solvent, therefore, other components of the electrolyte must have volatilized. The volatilization of iodine was suspected based on the formation of small crystals of iodine on container walls during treatment with heat and reduced pressure.

To eliminate the problem of variable iodine concentration, reference samples were made in which a solution of MEEP and the iodide salt were first dissolved in an organic solvent. A film of electrolyte was then deposited on the test cell electrodes as before, followed by treatment with heat and reduced pressure to remove all traces of solvent, subsequently confirmed by NMR spectroscopy. The sample was then exposed to a fixed amount of iodine vapor within a sealed container until a homogeneous mixture had formed and no non-absorbed iodine could be detected. The results are shown in Fig. 3 (sample 1N). The vapor-infused iodine system showed dramatically higher AC conductivity than the corresponding sample 1LVH (see Fig. 3) which was the product formed by solvent dissolution of

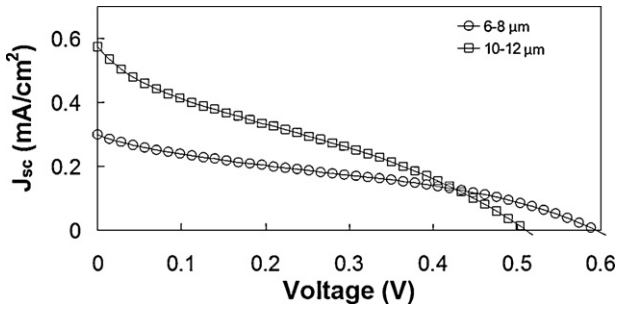

Fig. 4. *J–V* characteristics of nanocrystalline TiO_2 electrodes of different thickness. The electrolyte is composed of 1 M LiI, 0.5 M I_2, in MEEP dissolved in anhydrous acetonitrile. The electrolyte was drop-cast on sensitized TiO_2 films and was gently heated at 60 °C until all the solvents were removed (~10 min).

Table 2
Photovoltaic parameters of DSSCs of different nanocrystalline electrode thickness containing 1 M LiI, 0.5 M I_2, in MEEP dissolved in anhydrous acetonitrile.

Sample	V_{oc} (V)	J_{sc} (mA cm^{-2})	*ff*	P_{max} (mW)	η (%)
6–8 μm	0.59	0.29	0.32	0.014	0.056
10–12 μm	0.51	0.55	0.28	0.019	0.077

iodine into the electrolyte mixture followed by the application of heat and vacuum. At the same time, both conductivities are lower than those of samples in which residual solvents were detectable by NMR. This suggests that at least some of the loss of conductivity, and thus reduced cell efficiency, is probably due to iodine loss during the solvent removal procedures. Apart from the loss of signals corresponding to the solvent, NMR spectra of the polymer show no detectable change after removal of the solvent. This confirms that the changes that occur during the solvent removal process are not due to thermal decomposition of the MEEP polymer.

3.4. Electrolyte infiltration and heat treatment of cells

Because MEEP is a low T_g thermoplastic polymer, electrolyte infiltration into a nanoporous electrode should increase with temperature. Consequently, if all other variables remain constant, then the short-circuit current density and efficiency of a polymer electrolyte cell should increase following thermal treatment. An experimental investigation of this prospect was based on the photovoltaic properties of electrodes in two separate sets of experiments.

a. *Unsealed cells.* The first set focused on the limited infiltration ability of the polymer components. This set utilized TiO_2 nanocrystalline (nanosphere) film electrodes of different thickness, assembled with the same polymer electrolyte using the same procedure. The results reported in Fig. 4 and Table 2 show that, as the thickness of the TiO_2 film increases, an increase of the J_{sc} occurs, but that there is a sharp decrease in the voltage. The data also demonstrate that a device with a thicker TiO_2 nanosphere film suffers a lower fill factor and also lower V_{oc}, than devices with thin TiO_2 films. This is consistent with both a poor electrolyte–dye interface, and a slower transport of the redox couple in MEEP electrolytes. This last factor increases the internal resistance of the DSSC. As in DSSCs that utilize liquid electrolytes, as the thickness of the TiO_2 nanosphere film increases, so does the dark current, thus lowering the V_{oc}. These data support the observed trend that increasing cell thickness increases J_{sc} while also causing a decrease in the fill factor.

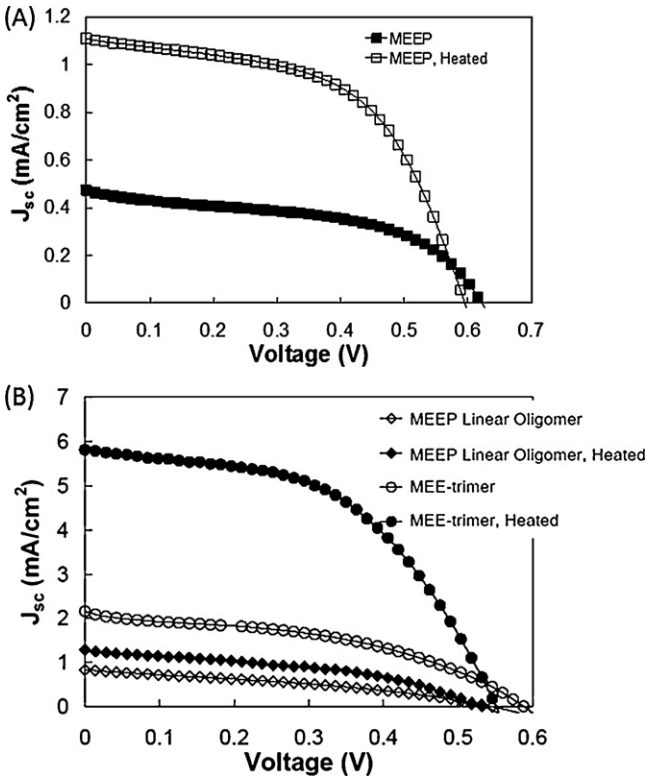

Fig. 5. *J–V* characteristics of DSSCs containing three phosphazene based electrolytes before and after heating at 60 °C. (a) MEEP polymer electrolyte is composed of 30:3:100:10 PMII:I_2:MEEP:tBuPy. No organic solvent was used, instead it was force-mixed through mechanical stirring. (b) Low molecular weight linear MEEP (MEEP-oligomer) and MEE trimer. They both contain 1 M LiI, 0.25 M I_2 and 0.5 M tBuPy. All data points shown here are averages for 2 experiments except 4N: thus error bars are not included.

b. *Sealed cells.* The second set of experiments involved *the post-assembly* heating of the cell, in which the cells were assembled, sealed, and tested for efficiency under normal conditions consistent with the samples mentioned above. The assembled cells were then placed in an oven at 60 °C for 1 h, allowed to return to room temperature, and tested again for power conversion efficiency. This experiment was intended to eliminate heat-induced changes in electrolyte composition as well as to assess the thermal stability of the overall cell assembly. The photovoltaic measurements for various samples are shown in Fig. 5 and Table 3. The baseline sample used in this case is the linear high polymeric MEEP sample (see Fig. 5 caption for details) with the PMII ionic liquid used as the iodide source to increase

Table 3
Photovoltaic parameters of DSSCs containing MEEP high polymer, MEEP linear oligomer, and MEE trimer electrolytes.

Sample	V_{oc} (V)	J_{sc} (mA cm^{-2})	*ff*	P_{max} (mW)	η (%)
MEEP before heating	0.63 ± 0.01	0.5 ± 0.2	0.51 ± 0.01	0.04 ± 0.01	0.15 ± 0.04
MEEP after heating	0.61 ± 0.02	1.1 ± 0.7	0.57 ± 0.02	0.09 ± 0.05	0.4 ± 0.2
MEEP oligomer before heating	0.55	0.8	0.35	0.04	0.16
MEEP oligomer after heating	0.54	1.0	0.42	0.07	0.28
MEE trimer before heating	0.58 ± 0.01	2.1 ± 0.5	0.43 ± 0.02	0.13 ± 0.04	0.5 ± 0.2
MEE trimer after heating	0.551 ± 0.005	5.8 ± 0.6	0.5082 ± 0.0002	0.41 ± 0.05	1.6 ± 0.2

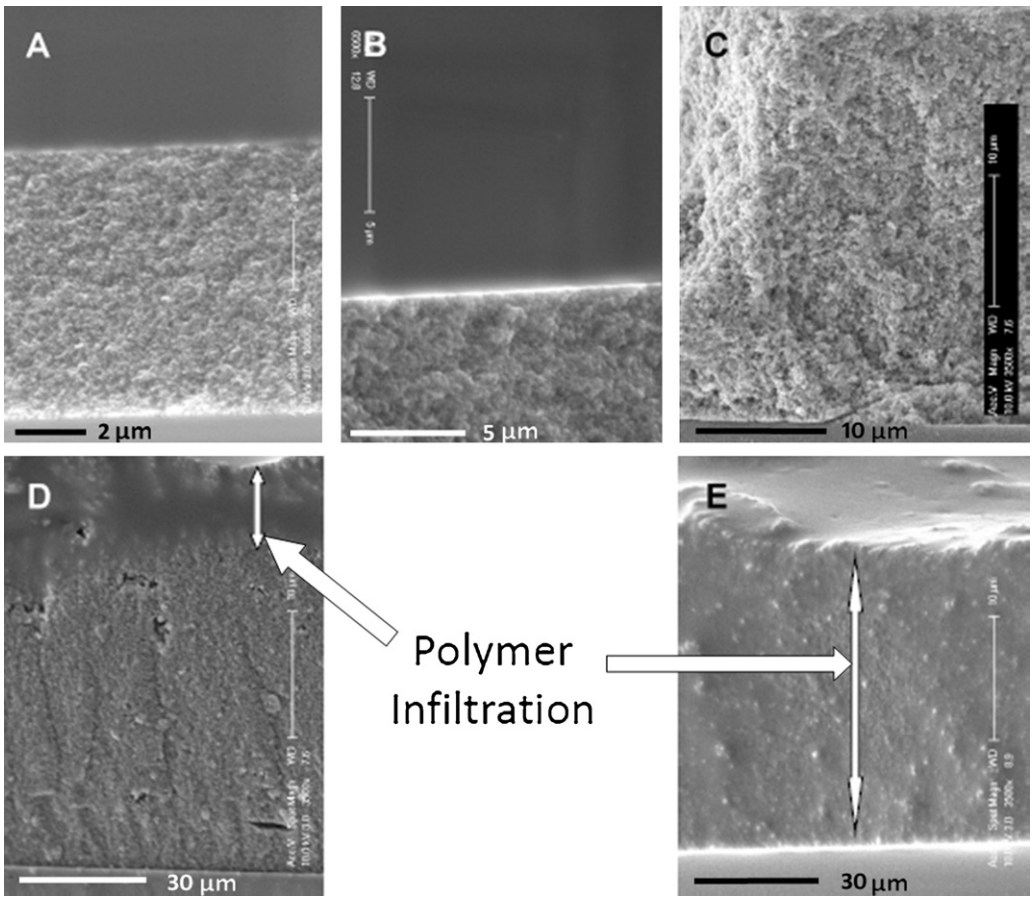

Fig. 6. Cross-sectional SEM images of polymer-infiltrated nanoparticle TiO_2 structures. (A) Solid polymer applied directly onto the TiO_2 layer. (B) Solid polymer melt-cast onto the TiO_2 surface. (C) Solution-cast polymer using acetone. (D) Combination of solution casting and 1 hour heating. (E) Combination of solution casting and 16 h heating. The arrows indicate the depth of infiltration.

ionic mobility and induce solvent-less mixing. This is compared with an electrolyte sample composed of low molecular weight (5 repeating units) linear MEEP oligomer **(1)** which is fluid at room temperature. The cyclic small-molecule liquid analogue, MEE trimer **(2)**, was also used as a comparison, the ionic conductivity of which was experimentally determined through the impedance method to be 9.53×10^{-5} S cm^{-1} as described earlier. The efficiency results for various samples are shown in Fig. 5. All the cells tested showed a marked increase in efficiency after 1 h of heat treatment, which supports the assumption of a heat-induced increase in electrolyte infiltration. It was expected that the MEEP linear oligomer would give a better photovoltaic performance than MEE trimer or MEEP high polymer because a liquid small molecule with a linear architecture should infiltrate the pores of TiO_2 films better than a long chain macromolecular system or, indeed, a cyclic molecule. However, it is suspected that the mass transport of the redox couple in the linear MEEP oligomer is slower than in MEE trimer due to the higher viscosity of the linear oligomer. In addition, the liquid MEE trimer was able to dissolve iodide salts and solid iodine without the assistance of solvents, which eliminated the influence of organic solvents on both ion mobility and electrolyte infiltration. None of these cells showed any visible failure after heat treatment, which implies that any volatile components remaining in the cell assembly did not generate sufficient vapor pressure to cause physical damage or leaks in the cell. Because such damage is one of the major concerns for liquid electrolyte dye-based cells, these results imply a significant advantage for the use of phosphazene electrolytes in practical solar cells.

3.5. Cross-section SEM examination of electrode–electrolyte assemblies

An alternative method to investigate the infiltration of polymers into a surface structure is through microscopic imaging of the electrode cross-sections after assembly with the electrolyte component. This method has been used in the past to detect the infiltration capacities of solid small molecule hole-conducting species in DSSCs [36]. Those results showed that such methods are effective for visualizing partial pore-filling effects [36]. In our case, a modification of the method was necessary due to the specific challenges for this system. For liquid electrolytes the cross section method was obviously inappropriate because of the fluidity of the infiltrate but, even for gum-type polymers such as MEEP, the act of cross-section fracture inevitably leads to elongation of the polymer layer and the formation of "overhangs" that interfere with observation. For this reason, after infusion into the electrode surface, the MEEP samples in this experiment were first strengthened through gamma-radiation crosslinking, and cross-sections were then obtained using freeze-fracture at liquid nitrogen temperatures.

The results for infiltration into nanosphere electrode surfaces are shown in Fig. 6. By comparing the images, it is apparent that the no-solvent introduction of MEEP as well as solvent-assisted assembly of MEEP at room temperature led to cross sections with a large fraction of open pores, which indicates poor electrolyte infiltration. As heat treatment was carried out, areas were observed in which the polymer infiltrated the nanoporous electrodes and resulted in composite-like filled structures that spread from the

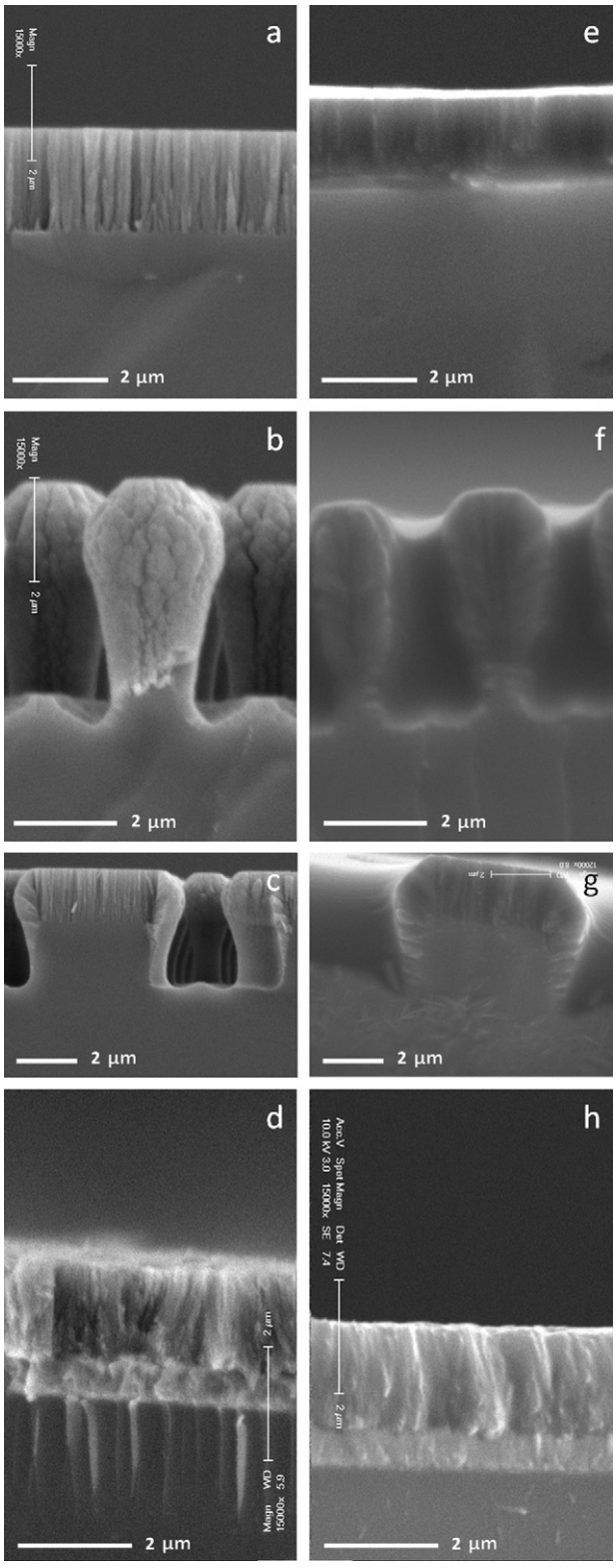

Fig. 7. Cross sectional images of various column electrodes before (a–d) and after (e–h) polymer infiltration. Samples are fabricated using oblique angle deposition [28] and using hydrothermal methods [35].

direction of polymer application. An increase in the time of the heat treatment gradually increased the pore filling percentage, until it reached 100% at 16 h. This demonstrated the effect of both heat and solvent-assisted electrolyte infiltration. The results also agree with the cell efficiency studies where the increase in efficiency by post-assembly heating was assumed to be related to improved pore filling by the electrolyte species.

3.6. Effect of column-type electrodes

SEM studies of the type described above were also applied to the various column-type structures fabricated by oblique angle deposition and thermochemical growth [28,35]. This variation of the e-beam and chemical deposition technique allowed the fabrication of a wide variety of structures ranging from wide stubs to brushes and narrow nanowires. Some examples of electrode structures fabricated through this method are shown in Fig. 7a–d. The sets of columns were designed to vary in diameter as well as spacing to examine their influence on electrolyte infiltration. A cross-sectional SEM after infiltration is shown in Fig. 7e–h. The degree of pore filling is higher for the columnar structures than for conventional nanosphere film electrodes, even for room temperature filling. There was no discernable difference between samples with different column-to-column distances, which may simply be due to the restrictions of the current column heights, which are 2 μm for narrow samples and 5 μm for wide ones.

4. Conclusions

At room temperature, the high polymeric electrolyte behaves in a similar way to a few other ion-transport polymeric systems, but fine-tuning of the polyphosphazene structure is expected to improve the performance. Understanding the ion conduction mechanism will require characterization of the individual ion mobilities, which we plan to investigate in the future.

The filling of nanoporous surface structures by MEEP polymer molecules gave the best results when a combination of solvent assistance and heat-fluidization processing was applied, as demonstrated by both the cross-sectional imaging as well as the post-assembly heat treatment experiments. Although simple heating was insufficient to promote full infiltration, it did play a major role. As with most melt-processing experiments, longer heating times led to higher degrees of infiltration. The characteristics of the high molecular weight thermoplastic polymer MEEP are particularly apparent when compared to the small-molecule based studies [36]. In the case of our polymer electrolytes, the gradual improvement in pore filling develops in a top-down fashion, with the face exposed to the electrolyte solution showing high polymer content, and with the degree of infiltration decreasing deeper into the surface structure. In contrast, a small-molecule study by Gratzel [36] showed relatively even, if incomplete, infiltration of the material within the nanoporous structure. As void spaces and incomplete infiltration are reasonable outcomes for film casting based on spin-casting and solution evaporation techniques, it is reasonable for the small molecule system to show infiltration patterns that differ from the results of melt-processing.

The disadvantage of thermal processing before cell assembly is the high probability of changes in electrolyte composition. This is supported by the fact that no differences in NMR spectra have been detected for pre- and post-heat treatment samples other than the loss of solvent. However, the loss of solvent may not be the only factor. The volatility of iodine is also a concern. The observations in this study did not reveal any problems for assembled cells, although quantitative studies using different cell-sealing processes will be necessary for assembly of a practical cell construct.

Titanium dioxide column structures show promise for allowing improved polymer infiltration into the electrodes, especially under room temperature conditions. Although the 2 μm limit for feature sizes using our current fabrication methods does not allow for a full comparison to be made with the thickness of nanocrystalline

layers (which are generally more than 10 μm thick) it does give a qualitative illustration of the effect of nano-columns on infiltration. Even when the spacing between columns is similar to the pore size in nanoparticle structures, an improvement in infiltration is still obvious. One of the main reasons could be that the straight-line channels provided by the channels between columns can provide a shorter pathway for the polymer to penetrate deep into the electrode. Moreover, the columns generate open channels as opposed to restricted pores with limited openings. Thus, infiltration is not hindered by trapped solvent or vapor in dead-end nanopores, and multiple directions for the polymer flow are facilitated. With taller columns it may be possible to achieve larger differences between the solvent removal methods and structure variations.

Use of the small molecule linear and cyclic analogues of MEEP facilitates infiltration into the electrode surfaces even when organic solvents are absent. The preliminary work with these media suggest that the ion mobility and cell efficiencies are lower for the small molecule electrolytes than for the solvent-cast high polymer, a result that is ascribed to traces of the organic carrier solvents remaining in the high polymer.

Acknowledgments

We thank the U.S. Department of Energy Golden Office (contract No. DE-FG36-08GO18011) for funding support. The fabrication of the low molecular weight electrolytes was assisted by Dr. Song-Yun Cho and Xiao Liu, while David Lee assisted with helpful discussions.

References

[1] A.L. Fahrenbruch, R.H. Bube, Fundamentals of Solar Cells, Academic Press, Inc., New York, NY, 1983, p. 576.
[2] L.L. Kazmerski, Renewable and Sustainable Energy Reviews 1 (1–2) (1997) 71–170.
[3] G.H. Lin, D.E. Carlson, International Journal of Hydrogen Energy 25 (2000) 807–811.
[4] W. Palz, H. Zibetta, International Journal of Solar Energy 10 (1991) 11–216.
[5] R.D. McConnell, Renewable and Sustainable Energy Reviews 6 (3) (2002) 271–293.
[6] J. Gartner, Wired News, 2005, March 28.
[7] D.E. Carlson, C.R. Wronski, Applied Physics Letters 28 (11) (1976) 671–673.
[8] R.B. Bergmann, Applied Physics A: Materials Science and Processing 69 (2) (1999) 187.
[9] G.A. Chamberlain, Solar Cells 8 (1983) 47–83.
[10] W.U. Huynh, J.J. Dittmer, A.P. Alivisatos, Science 295 (5564) (2002) 2425–2427.
[11] M. Gratzel, Journal of Photochemistry and Photobiology C: Photochemistry Reviews 4 (2003) 145–153.
[12] B. O'Regan, M. Gratzel, Nature 353 (1991) 737.
[13] (a) C.Y. Chen, M.K. Wang, J.Y. Li, N. Pootrakulchote, L. Alibabai, C. Ngoc-le, Ha. Decoppet, J.D. Tsai, J.H. Gratzel, C.G Wu, S.M. Zakeeruddin, M. Graetzel, ACS Nano 3 (10) (2009) 3103–3109;
(b) N.R. Neale, N. Kopidakis, J. Lagemaat, M. Gratzel, A.J. Frank, Journal of Physical Chemistry B 1090 (2005) 12485.
[14] A. Baumann, Y. Bhargava, Z.X. Liu, G. Nemet, J. Wilcox, Materials Science and Engineering/C226 (2004).
[15] G. Smestad, Solar Energy Materials and Solar Cells 32 (1994) 259–273.
[16] M. Grätzel, Journal of Photochemistry and Photobiology A: Chemistry 164 (1–3) (2004) 3–14.
[17] M. Gorlov, L. Kloo, Dalton Transactions 20 (2008) 2655–2666.
[18] A.F. Nogueira, C. Longo, M.A. De Paoli, Coordination Chemistry Reviews 248 (13–14) (2004) 1455–1468.
[19] A.F. Nogueira, J.R. Durrant, M.A. De Paoli, Advanced Materials 13 (11) (2001) 826–830.
[20] P. Wang, S.M. Zakeeruddin, J.E. Moser, M.K. Nazeeruddin, T. Sekiguchi, M. Gratzel, Nature Materials 2 (2003) 402–498.
[21] W. Kubo, S. Kambe, S. Nakade, T. Kitamura, K. Hanabusa, Y. Wada, S. Yanagida, Journal of Physical Chemistry B 107 (2003) 4374–4381.
[22] J.H. Kim, M.S. Kang, Y.J. Kim, J. Won, N.G. Park, Y.S. Kang, Chemical Communications (2004) 1662–1663.
[23] H. Yang, C. Yu, Q. Song, Y. Xia, F. Li, Z. Chen, X. Li, T. Yi, C. Huang, Chemistry of Materials 18 (22) (2006) 5173–5177.
[24] P.M. Blonsky, D.F. Shriver, P. Austin, H.R.J. Allcock, Journal of the American Chemical Society 106 (22) (1984) 6854–6855.
[25] H.R. Allcock, P.E. Austin, T.X. Neenan, J.T. Sisko, P.M. Blonsky, D.F. Shriver, Macromolecules 19 (6) (1986) 1508–1512.
[26] H.R. Allcock, S.R. Pucher, M.L. Tumer, R. Fitzpatrick, Journal of Macromolecules 25 (1992) 5513–5521.
[27] W.U. Huynh, J.J. Dittmer, A.P. Alivisatos, Science 295 (2002) 2425.
[28] M.W. Horn, M.D. Pickett, R. Messier, A. Lakhtakia, Journal of Vacuum Science Technology B 22 (6) (2004) 3426–3430.
[29] F. Li, F. Cheng, J. Shi, F. Cai, M. Liang, J. Chen, Journal of Power Sources 165 (2007) 911–915.
[30] S.T. Fei, H.R. Allcock, Journal of Power Sources 195 (2010) 2082–2088.
[31] P.M. Blonsky, D.F. Shriver, P.E. Austin, H.R. Allcock, Journal of the American Chemical Society 106 (1984) 6854.
[32] C.H. Honeyman, I. Manners, C.T. Morrissey, H.R. Allcock, Journal of the American Chemical Society 117 (1995) 7035.
[33] J. Paulsdorf, M. Burjanadze, K. Hagelschur, H.-D. Wiemhofer, Solid State Ionics 169 (2004) 25–33.
[34] S.-H.A. Lee, N.M. Abrams, P.G. Hoertz, G.D. Barber, L.I. Halaoui, T.E. Mallouk, Journal of Physical Chemistry B 112 (2008) 14415–14421.
[35] X. Feng, K. Shankar, O.K. Varghese, M. Paulose, T.J. LaTempa, C.A. Grimes, Nano Letters 8 (11) (2008) 3781–3786.
[36] H.J. Snaith, R. Humphry-Baker, P. Chen, I. Cesar, S.M. Zakeeruddin, M. Gratzel, Nanotechnology 19 (424003) (2008) 12.